

Theory of fermion exchange in massive quantum electrodynamics at high energy.

II. Sixth-order perturbation theory*

Barry M. McCoy[†]

The Institute for Theoretical Physics, State University of New York at Stony Brook, Stony Brook, New York 11794

Tai Tsun Wu

Gordon McKay Laboratory, Harvard University, Cambridge, Massachusetts 02138

(Received 4 August 1975)

In this paper we present the details of our sixth-order perturbation theory calculation of the high-energy behavior of Compton scattering near the backward direction and pair annihilation. For each of these matrix elements, a formula is obtained not only for the leading term, which is real, but also for the leading imaginary part. Momentum-space techniques are used throughout. In particular we impose a cutoff in the transverse momentum and then compute the behavior as s (the square of the center-of-mass energy) $\rightarrow \infty$. With this procedure there are 3 Feynman diagrams which contribute to the leading real part. These 3 diagrams each give a factor of $\ln^2 s$ and an integral over transverse-momentum space. Each of these 3 transverse integrals separately diverge as $k_{\max} \rightarrow \infty$ but when added together the $k_{\max} \rightarrow \infty$ limit may be taken and the result agrees with the result previously obtained by Feynman parameters. To complete the evaluation of the leading imaginary part a fourth diagram is needed.

I. INTRODUCTION

In this paper we consider in sixth-order perturbation theory the processes of Compton scattering near the backward direction and pair annihilation in the quantum field theory of vector mesons of mass λ (called photons, γ) interacting with a conserved current of spin- $\frac{1}{2}$ fermions of mass m (called electrons and positrons, e^- and e^+). The kinematics of these two reactions are given in Fig. 1. We will study these two related processes in the high-energy limit, where

$$s = (\gamma_2 + \gamma_3)^2 \rightarrow \infty \tag{1.1}$$

and

$$t = (2\gamma_1)^2 \leq 0 \tag{1.2}$$

is fixed. [We use the metric (+---).] In addition we always restrict ourselves to the case where the vector meson is polarized in the transverse direction in the center-of-mass system.

In this limit the sixth-order amplitudes are known¹ to have the order of magnitude $s^{1/2} \ln^2 s$. The factor of $s^{1/2}$ arises from the fact that the electron has spin $\frac{1}{2}$. It comes from the spinors of the initial and final electron in the case of backward Compton scattering and from the spinors of the initial electron and positron in the case of pair annihilation. Because this factor of $s^{1/2}$ is kinematic in origin and is present (implicitly via spinors) in every amplitude we write down, we will suppress it in all further discussions.

The sixth-order pair-annihilation amplitude (after the kinematic factor $s^{1/2}$ is removed) has a discontinuity in s (considered as a complex vari-

able) both across the positive- s axis and across the negative- s axis for sufficiently large $|s|$ (in contrast to the fourth-order annihilation amplitude which only has a cut for $s > 4m^2$). We are interested in both of these discontinuities, and to study them both we need two pieces of information as $s \rightarrow \infty$. Loosely speaking, we take these two pieces of information to be the real and imaginary parts of the scattering amplitude (where for this purpose

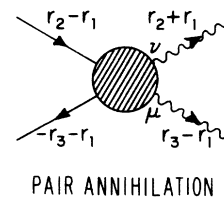
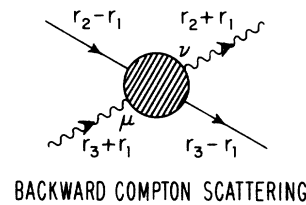


FIG. 1. Kinematics of the reactions of Compton scattering near the backward direction and pair annihilation. The incoming particles are on the left-hand side and the outgoing particles are on the right-hand side.

all spinors and γ matrices are treated as real).

It is the purpose of this paper to study in sixth order both the real and imaginary parts of the scattering amplitude for Compton scattering near the backward direction, or equivalently that of pair annihilation. The real part for both processes is of order $\ln^2 s$ and the imaginary part is of order $\ln s$. The physics of our result has been discussed previously.² Here we restrict our attention solely to the details of the calculation.

The real parts of these amplitudes have been studied previously^{1,3} by use of Feynman parameters. The procedure of Ref. 1, although correct, is technically very cumbersome to use and it would be an act of madness to carry out such a calculation to higher orders of perturbation theory. However, we have also seen that in the case of elastic scattering that momentum-space techniques⁴ prove to be much more efficient in extracting the leading-order asymptotic behavior than were the Feynman-parameter methods.⁵ Therefore, since our goal is to extend the previous work to higher orders we will in this paper, in addition to computing the leading imaginary part, redo the calculation of the real part by use of momentum-space techniques. We will present sixth-order calculations in considerable detail. In succeeding papers we will use these techniques in a more summary fashion.

The utility of momentum space stems from the fact that individual Feynman diagrams have an asymptotic behavior which is larger ($\ln^3 s$ in sixth order) than that of the complete amplitude itself ($\ln^2 s$ in sixth order). When using Feynman parameters there is not much we can do about this. However, in momentum space, calculations may be simplified and the number of contributing diagrams reduced by adopting the following procedure. First of all, we use the coordinate system in which the spacial component of r_2 has magnitude ω and lies in the direction of the z axis while the spatial component of r_3 also has magnitude ω but lies in the direction of the negative- z axis. We are interested in the limiting behavior as $\omega \rightarrow \infty$. Then

$$r_2 = (\omega + O(1/\omega), \omega, 0), \quad (1.3a)$$

$$r_3 = (\omega + O(1/\omega), -\omega, 0), \quad (1.3b)$$

$$r_1 = (O(1/\omega), O(1/\omega), \vec{r}_\perp), \quad (1.3c)$$

and the invariants are

$$\begin{aligned} s &\sim 2r_3 \cdot r_2 \\ &\sim (2\omega)^2 \end{aligned} \quad (1.4)$$

and

$$t \sim -4\vec{r}_\perp^2. \quad (1.5)$$

[We use the notation for components of a four-vector p of $(p_0, p_3, \vec{p}_\perp)$, where \vec{p}_\perp is a two-vector in the x - y plane.] Secondly, in terms of this coordinate system all integrals over x and y components of the momenta [called collectively transverse (\perp) components] are cut off at some k_{\max} independent of ω . For each separate diagram the $s \rightarrow \infty$ behavior with the cutoff will in general not be the same as the behavior without the cutoff. In particular, for sixth order no diagram will have a cutoff $s \rightarrow \infty$ behavior of order greater than $\ln^2 s$. Only after the diagrams are added together is the cutoff allowed to go to infinity.

This procedure involves, in effect, an interchange of the limits $\lim_{s \rightarrow \infty}$ and $\lim_{k_{\max} \rightarrow \infty}$. Since we do not have a mathematical proof that this interchange does not affect the high-energy results, it is a further purpose of this paper to show that this method of calculation does indeed give the same asymptotic behavior for the real part as was previously calculated using the more rigorous Feynman-parameter method. This gives us confidence that the same interchange of limits will lead to the correct asymptotic behavior in higher orders of perturbation theory.

The outline of the paper is as follows. In Sec. II we provide some orientation by calculating the leading real and imaginary parts in the fourth-order perturbation theory. In Sec. III we give a short discussion of the three diagrams that contribute to the leading real part in sixth order. The leading real and imaginary part of these diagrams are then individually computed in Secs. IV, V, and VI. We then add these three amplitudes together in Sec. VII. In Sec. VIII we introduce a device called a "momentum-flow diagram" which will prove to be of great utility in simplifying the labor of the momentum-space calculations. In Sec. IX we use these momentum-flow diagrams to compute the additional diagram needed to obtain the complete leading-order behavior for the imaginary part of the amplitude. The final answer is given by (9.21).

A word is needed about our notation. The amplitude for pair annihilation is denoted by $\overline{\mathfrak{M}}_{\mu\nu}(s, r_1)$, while the amplitude for backward Compton scattering is denoted by $\mathfrak{M}_{\mu\nu}(s, r_1)$. An amplitude in the $[2(n+1)]$ th order of perturbation theory is referred to as $\overline{\mathfrak{M}}_{\mu\nu}^{(n)}(s, r_1)$ and $\mathfrak{M}_{\mu\nu}^{(n)}(s, r_1)$, for pair annihilation and backward Compton scattering, respectively. Finally we define the symbol \doteq to mean that as $s \rightarrow \infty$ with t fixed in the $[2(n+1)]$ th order of perturbation theory, the real parts of order $\ln^n s$ on both sides of the symbol are equal and the imaginary parts of order $\ln^{n-1} s$ on both sides of the symbol are equal. For example, in $[2(n+1)]$ th order

$$\ln^n s \doteq \ln^n s + \ln^{n-1} s \quad (1.6)$$

but it is not true that

$$\ln^n s \doteq \ln^n s + i \ln^{n-1} s. \quad (1.7)$$

II. FOURTH-ORDER PERTURBATION THEORY

For orientation we will, in this section, study the behavior of the fourth-order Feynman diagrams of Figs. 2 and 3. These are the only fourth-order diagrams that contribute to leading order as $s \rightarrow \infty$.

First consider the pair-annihilation diagram of Fig. 2. This has the amplitude

$$\bar{\mathcal{M}}_{\mu\nu}^{(1)}(s, r_1) = i g^4 \int d^4 k (2\pi)^{-4} [N_1^{(1)}]_{\mu\nu} D_1^{(1)-1}, \quad (2.1)$$

where

$$\begin{aligned} D_1^{(1)} &= (k^2 - \lambda^2 + i\epsilon) [(r_2 - r_1 - k)^2 - m^2 + i\epsilon] \\ &\quad \times [(2r_1 + k)^2 - m^2 + i\epsilon] \\ &\quad \times [(r_3 + r_1 + k)^2 - m^2 + i\epsilon] \end{aligned} \quad (2.2)$$

and

$$\begin{aligned} [N_1^{(1)}]_{\mu\nu} &= \bar{v}(r_3 + r_1) \gamma_\sigma (-\not{r}'_3 - \not{r}'_1 - \not{k} + m) \\ &\quad \times \gamma_\mu (-2\not{r}'_1 - \not{k} + m) \gamma_\nu \\ &\quad \times (\not{r}'_2 - \not{r}'_1 - \not{k} + m) \gamma_\sigma u(r_2 - r_1). \end{aligned} \quad (2.3)$$

To asymptotically expand (2.1) when s is large, we first consider the integral with $[N_1^{(1)}]_{\mu\nu}$ replaced by 1. This integral is conveniently studied when ω is large by introducing⁴

$$k_+ = k_0 + k_3, \quad (2.4a)$$

$$k_- = k_0 - k_3, \quad (2.4b)$$

with

$$\begin{aligned} D_1^{(1)} &= (k_+ k_- - \vec{k}_\perp^2 - \lambda^2 + i\epsilon) [(r_{2+} - r_{1+} - k_+) (r_{2-} - r_{1-} - k_-) - (\vec{r}_\perp + \vec{k}_\perp)^2 - m^2 + i\epsilon] \\ &\quad \times [(2r_{1+} + k_+) (2r_{1-} + k_-) - (2\vec{r}_\perp + \vec{k}_\perp)^2 - m^2 + i\epsilon] [(r_{3+} + r_{1+} + k_+) (r_{3-} + r_{1-} + k_-) - (\vec{r}_\perp + \vec{k}_\perp)^2 - m^2 + i\epsilon], \end{aligned} \quad (2.8)$$

which, using (2.5)–(2.7), may be approximated as

$$\begin{aligned} D_1^{(1)} \sim \bar{D}_1^{(1)} &= (k_+ k_- - \vec{k}_\perp^2 - \lambda^2 + i\epsilon) [(k_+ - 2\omega) k_- - (\vec{r}_\perp + \vec{k}_\perp)^2 - m^2 + i\epsilon] \\ &\quad \times [k_+ k_- - (2\vec{r}_\perp + \vec{k}_\perp)^2 - m^2 + i\epsilon] [k_+ (2\omega + k_-) - (\vec{r}_\perp + \vec{k}_\perp)^2 - m^2 + i\epsilon]. \end{aligned} \quad (2.9)$$

After this basic approximation we evaluate the k_+ integral by means of contour integration. The zeros of (2.9) are at

$$k_+ = k_-^{-1} (\vec{k}_\perp^2 + \lambda^2 - i\epsilon), \quad (2.10a)$$

$$k_+ = 2\omega + k_-^{-1} [(2\vec{r}_\perp + \vec{k}_\perp)^2 + m^2 - i\epsilon], \quad (2.10b)$$

$$k_+ = k_-^{-1} [(2\vec{r}_\perp + \vec{k}_\perp)^2 + m^2 - i\epsilon], \quad (2.10c)$$

and

$$k_+ = (2\omega + k_-)^{-1} [(\vec{r}_\perp + \vec{k}_\perp)^2 + m^2 - i\epsilon]. \quad (2.10d)$$

If $k_- > 0$, then all these poles of the integrand are in the lower half of the k_+ plane and, since the integrand

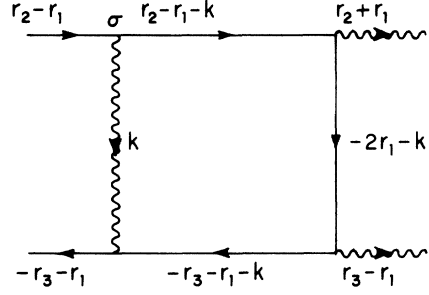


FIG. 2. The only fourth-order Feynman diagram for pair annihilation that contributes to leading order in the limit $(r_2 + r_3)^2 = s \rightarrow \infty$.

$$dk_0 dk_3 = \frac{1}{2} dk_+ dk_-. \quad (2.4c)$$

We note that

$$\begin{aligned} r_{2+} &= r_{20} + r_{23} \\ &= 2\omega + O\left(\frac{1}{\omega}\right), \end{aligned} \quad (2.5a)$$

$$\begin{aligned} r_{2-} &= r_{20} - r_{23} \\ &= O\left(\frac{1}{\omega}\right), \end{aligned} \quad (2.5b)$$

$$r_{3+} = O\left(\frac{1}{\omega}\right), \quad (2.6a)$$

$$r_{3-} = 2\omega + O\left(\frac{1}{\omega}\right), \quad (2.6b)$$

and

$$r_{1\pm} = O\left(\frac{1}{\omega}\right). \quad (2.7)$$

With these coordinates we may rewrite (2.2) as

vanishes like k_+^{-4} at infinity the contour may be closed in the upper half plane to give zero. Likewise, if $k_- < -2\omega$, all poles are in the upper half plane and the integral is again zero. Therefore, to get a non-zero contribution to the k_+ integral we must have

$$-2\omega < k_- < 0. \quad (2.11)$$

When this holds we may close the contour of integration on the one pole which is in the lower half plane, namely (2.10d), and we find

$$\begin{aligned} \int d^4k \bar{D}_1^{-1} = & -\pi i \int d^2\vec{k}_\perp \int_{-2\omega}^0 dk_- (2\omega + k_-)^{-1} \{k_- (2\omega + k_-)^{-1} [(\vec{r}_\perp + \vec{k}_\perp)^2 + m^2 - i\epsilon] - \vec{k}_\perp^2 - \lambda^2 + i\epsilon\}^{-1} \\ & \times \left\{ -k_- \left[2\omega - \frac{(\vec{r}_\perp + \vec{k}_\perp)^2 + m^2 - i\epsilon}{2\omega + k_-} \right] - (\vec{r}_\perp + \vec{k}_\perp)^2 - m^2 + i\epsilon \right\}^{-1} \\ & \times \{k_- (2\omega + k_-)^{-1} [(\vec{r}_\perp + \vec{k}_\perp)^2 + m^2 - i\epsilon] - (2\vec{r}_\perp + \vec{k}_\perp)^2 - m^2 + i\epsilon\}^{-1}. \end{aligned} \quad (2.12)$$

We proceed further by approximately evaluating the k_- integral. When k_- is approximately -2ω we may replace k_- by -2ω except in the factors $2\omega + k_-$. The resulting integral converges at $k_- = -2\omega$. Therefore this end of the integration range does not give any factors of $\ln\omega$. Therefore we may consider ω to be much larger than $|k_-|$ and hence (2.12) is approximated by

$$-\pi i \int d^2\vec{k}_\perp (2\omega)^{-1} (\vec{k}_\perp^2 + \lambda^2)^{-1} [(2\vec{r}_\perp + \vec{k}_\perp)^2 + m^2]^{-1} \int_{-2\omega}^0 dk_- [-2\omega k_- - (\vec{r}_\perp + \vec{k}_\perp)^2 - m^2 + i\epsilon]^{-1}. \quad (2.13)$$

As $\epsilon \rightarrow 0$ there is a singularity on the integration path at

$$-k_- = (2\omega)^{-1} [(\vec{r}_\perp + \vec{k}_\perp)^2 + m^2]. \quad (2.14)$$

Therefore this integral has an imaginary as well as a real part and we find

$$\begin{aligned} \int_{-2\omega}^0 dk_- [-2\omega k_- - (\vec{r}_\perp + \vec{k}_\perp)^2 - m^2 + i\epsilon]^{-1} &= (2\omega)^{-1} \ln \frac{(2\omega)^2 - (\vec{r}_\perp + \vec{k}_\perp)^2 - m^2 + i\epsilon}{-(\vec{r}_\perp + \vec{k}_\perp)^2 - m^2 + i\epsilon} \\ &\sim (2\omega)^{-1} [\ln(4\omega^2) - \pi i]. \end{aligned} \quad (2.15)$$

This evaluation is correct to leading order in $\ln\omega$ for both the real *and* the imaginary part (even though the imaginary part is smaller than the real part by a power of $\ln\omega$). Using (2.15) in (2.13) we find that, correct to leading order,

$$\begin{aligned} iS \int d^4k (k^2 - \lambda^2 + i\epsilon)^{-1} [(r_2 - r_1 - k)^2 - m^2 + i\epsilon]^{-1} [(2r_1 + k)^2 - m^2 + i\epsilon]^{-1} [(r_3 + r_1 + k)^2 - m^2 + i\epsilon]^{-1} \\ \doteq \pi (\ln\omega - \pi i) \int d^2\vec{k}_\perp (\vec{k}_\perp^2 + \lambda^2)^{-1} [(2\vec{r}_\perp + \vec{k}_\perp)^2 + m^2]^{-1}. \end{aligned} \quad (2.16)$$

We turn now to the approximation of the numerator (2.3). Because $k_- = o(\omega)$ was the only region of k_- space that contributed significantly to the leading-order result (2.16) and because the k_+ pole we closed on (2.10d) is also $o(\omega)$ we approximate $[N_1^{(1)}]_{\mu\nu}$ by dropping k when compared with either r_2 or r_3 . Therefore

$$\begin{aligned} [N_1^{(1)}]_{\mu\nu} \sim & \bar{v}(r_3 + r_1) \gamma_\sigma (-\not{r}_3) \gamma_\mu (-2\not{r}_1 - \not{k} + m) \\ & \times \gamma_\nu \not{r}_2 \gamma_\sigma u(r_2 - r_1). \end{aligned} \quad (2.17)$$

Now the Dirac equations for the free spinors $u(r_2 - r_1)$ and $v(r_3 + r_1)$ are

$$(\not{r}_2 - \not{r}_2 - m)u(r_2 - r_1) = 0 \quad (2.18a)$$

and

$$(\not{r}_3 + \not{r}_1 + m)v(r_3 + r_1) = 0. \quad (2.18b)$$

Therefore we anticommute \not{r}_2 to the right and \not{r}_3 to the left, using the anticommutation relation

$$\{\gamma_\mu, \gamma_\nu\} = 2g_{\mu\nu}, \quad (2.19)$$

and employ (2.18) to drop those terms where \not{r}_2 acts on $u(r_2 - r_1)$ or \not{r}_3 acts on $\bar{v}(r_3 + r_1)$. We obtain

$$\begin{aligned} [N_1^{(1)}]_{\mu\nu} \sim & -2\bar{v}(r_3 + r_1) \gamma_\mu (-2\not{r}_1 - \not{k} + m) \\ & \times \gamma_\nu \not{r}_2 \not{r}_3 u(r_2 - r_1) \\ \sim & -4r_2 \cdot r_3 \bar{v}(r_3 + r_1) \gamma_\mu (-2\not{r}_1 - \not{k} + m) \\ & \times \gamma_\nu u(r_2 - r_1). \end{aligned} \quad (2.20)$$

Now μ and ν are the vector indices of the polar-

ization vectors of the external photons. Because we have restricted our attention to polarizations which are transverse (in the center-of-mass frame) to the momentum of the photons r_2+r_1 or r_3-r_1 we may restrict the indices μ and ν to be x and y (called collectively \perp). With this restriction on μ and ν we see that to leading order \not{k} may be replaced by

$$\vec{k}_\perp = -\gamma_1 k_1 - \gamma_2 k_2 \quad (2.21)$$

because \not{k}_+ and \not{k}_- anticommute with γ_\perp and because by (2.18)

$$\not{k}_+ u(r_2 - r_1) = 0 \quad (2.22a)$$

and

$$\bar{v}(r_3 + r_1) \not{k}_- = 0 \quad (2.22b)$$

Therefore $[N_1^{(1)}]_{\mu\nu}$ is finally approximated as

$$[N_1^{(1)}]_{\mu\nu} \sim -4(r_2 \cdot r_3) \bar{v}(r_3 + r_1) \times \gamma_\mu (-2\vec{r}_\perp - \vec{k}_\perp + m) \gamma_\nu u(r_2 - r_1). \quad (2.23)$$

$$\begin{aligned} \overline{\mathfrak{M}}_{\mu\nu}^{(1)}(s, r_1) &\doteq \frac{g^4}{8\pi^3} (\ln s - \pi i) \int d^2 \vec{k}_\perp \frac{\bar{v}(r_3 + r_1) \gamma_\mu (2\vec{r}_\perp + \vec{k}_\perp - m) \gamma_\nu u(r_2 - r_1)}{(\vec{k}_\perp^2 + \lambda^2) [(2\vec{r}_\perp + \vec{k}_\perp)^2 + m^2]} \\ &= g^2 (\ln s - \pi i) \bar{v}(r_3 + r_1) \gamma_\mu \frac{1}{2\vec{r}_\perp + m} \alpha(2\vec{r}_\perp) \gamma_\nu u(r_2 - r_1), \quad (2.24) \end{aligned}$$

where

$$\begin{aligned} \alpha(2\vec{r}_\perp) &= \frac{g^2}{8\pi^3} (2\vec{r}_\perp + m) \\ &\times \int d^2 \vec{k}_\perp \frac{2\vec{r}_\perp + \vec{k}_\perp - m}{[(2\vec{r}_\perp + \vec{k}_\perp)^2 + m^2] (\vec{k}_\perp^2 + \lambda^2)}. \quad (2.25) \end{aligned}$$

This is the fourth-order result of Gell-Mann, Goldberger, Low, Marx, and Zachariasen.³

It is also instructive to consider explicitly the corresponding diagram for backward Compton scattering (Fig. 3). This amplitude is given by

$$\overline{\mathfrak{M}}_{\mu\nu}^{(1)}(s, r_1) = ig^4 \int d^4 k (2\pi)^{-4} [N_2^{(1)}]_{\mu\nu} D_2^{(1)-1}, \quad (2.26)$$

$$[N_2^{(1)}]_{\mu\nu} \sim 4(r_2 \cdot r_3) \bar{u}(r_3 - r_1) \gamma_\mu (-2\vec{r}_\perp - \vec{k}_\perp + m) \gamma_\nu u(r_2 - r_1). \quad (2.29)$$

The denominator is approximated by

$$\begin{aligned} \bar{D}_2 &= (k_+ k_- - \vec{k}_\perp^2 - \lambda^2 + i\epsilon) [(k_+ - 2\omega)k_- - (\vec{r}_\perp + \vec{k}_\perp)^2 - m^2 + i\epsilon] \\ &\times [k_+ k_- - (2\vec{r}_\perp + \vec{k}_\perp)^2 - m^2 + i\epsilon] [k_+ (k_- - 2\omega) - (\vec{r}_\perp + \vec{k}_\perp)^2 - m^2 + i\epsilon]. \quad (2.30) \end{aligned}$$

Now the k_+ integral is zero unless

$$0 < k_- < 2\omega \quad (2.31)$$

and we have

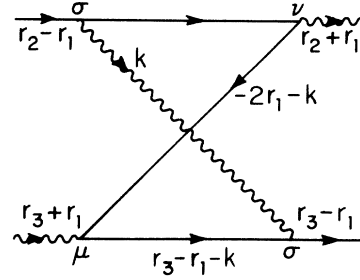


FIG. 3. The only fourth-order Feynman diagram for Compton scattering near the backward direction that contributes to leading order in the limit $(r_2 + r_3)^3 = s \rightarrow \infty$.

By now all dependence of $[N^{(1)}]_{\mu\nu}$ on k_+ and k_- has been approximated away. Therefore we may combine the result (2.16) with (2.23) to find that as $s = (2\omega)^2 \rightarrow \infty$ in fourth order

with

$$\begin{aligned} D_2^{(1)} &= (k^2 - \lambda^2 + i\epsilon) [(r_2 - r_1 - k)^2 - m^2 + i\epsilon] \\ &\times [(2r_1 + k)^2 - m^2 + i\epsilon] \\ &\times [(r_3 - r_1 - k)^2 - m^2 + i\epsilon] \quad (2.27) \end{aligned}$$

and

$$\begin{aligned} [N_2^{(1)}]_{\mu\nu} &= \bar{u}(r_3 - r_1) \gamma_\sigma (\not{r}'_3 - \not{r}'_1 - \not{k} + m) \\ &\times \gamma_\mu (-2\not{r}'_1 - \not{k} + m) \\ &\times \gamma_\nu (\not{r}'_2 - \not{r}'_1 - \not{k} + m) \gamma_\sigma u(r_2 - r_1). \quad (2.28) \end{aligned}$$

The numerator is approximated as

$$\int d^4k \bar{D}_2^{-1} = -\pi i \int d^2\vec{k}_\perp \int_0^{2\omega} dk_- (2\omega - k_-) [-k_- (2\omega - k_-)]^{-1} [(\vec{r}_\perp + \vec{k}_\perp)^2 + m^2 - i\epsilon]^{-1} [\vec{k}_\perp^2 - \lambda^2 + i\epsilon]^{-1} \times \left\{ -k_- \left[2\omega + \frac{(\vec{r}_\perp + \vec{k}_\perp)^2 + m^2 - i\epsilon}{2\omega - k_-} \right] - (\vec{r}_\perp + \vec{k}_\perp)^2 - m^2 + i\epsilon \right\}^{-1} \times [-k_- (2\omega - k_-)]^{-1} [(\vec{r}_\perp + \vec{k}_\perp)^2 + m^2 - i\epsilon]^{-1} [(2\vec{r}_\perp + \vec{k}_\perp)^2 - m^2 + i\epsilon]^{-1}. \tag{2.32}$$

The largest contribution again comes from the region $k_- = o(\omega)$ so we approximate (2.32) as

$$\int d^4k \bar{D}_2^{-1} \sim -\pi i \int d^2\vec{k}_\perp (\vec{k}_\perp^2 + \lambda^2)^{-1} [(2\vec{r}_\perp + \vec{k}_\perp)^2 + m^2]^{-1} (2\omega)^{-1} \int_0^{2\omega} dk_- [-2\omega k_- - (\vec{r}_\perp + \vec{k}_\perp)^2 - m^2 + i\epsilon]^{-1}. \tag{2.33}$$

Here, if $\epsilon = 0$ there is no pole on the path of integration and thus the integral is real. Therefore we find

$$\bar{\mathfrak{M}}_{\mu\nu}^{(1)}(s, r_1) \doteq \bar{u}(r_3 + r_1) g^2 \ln s \gamma_\mu \frac{1}{2\vec{r}_\perp + m} \times \alpha(2\vec{r}_\perp) \gamma_\nu u(r_2 - r_1). \tag{2.34}$$

As presented above, these two fourth-order calculations are very easy to do. Their ease stems from the fact that we have approximated the numerator and the denominator as early in the calculation as possible. Since the computations in higher orders of perturbation theory will be done in exactly the same fashion, the reader should be convinced at this point that the approximation scheme is valid. For example, if we do not approximate the denominator (2.8) by (2.9) before we integrate over k_+ , we find that instead of there being only one contributing region like (2.11) there are actually three contributing regions of k_- space which differ in which half plane the k_+ poles lie in. One of these regions approaches (2.11) as $\omega \rightarrow \infty$. The other two have widths of $O(1/\omega)$. It is particularly important to realize that these "little" regions cannot give a contribution of order $\omega^{-2} \ln \omega$. Loosely speaking, the contribution from such a "little" region appears to be small by a power of ω . On the other hand, the process of integration may restore a power of ω . But if an integral is used to restore a lost power of ω it can no longer be used to produce a power of $\ln \omega$. Hence all terms omitted are down by at least a power of $\ln \omega$. The reader should be warned, however, that this approximation is quite delicate and must not be applied blindly.

Finally, we remark that there are no other fourth-order Feynman diagrams as large as the ones computed above.

III. SIXTH-ORDER DIAGRAMS WITH A REAL PART OF ORDER $\ln^2 s$

In fourth order it made no difference whether or not we used a cutoff in the \vec{k}_\perp integration since

there was only one contributing diagram and since the resulting two-dimensional integral (2.25) converges when the cutoff is removed. The situation changes in sixth order.

We commence the study of the sixth order by considering the three diagrams of Fig. 4. These are the only diagrams that contribute to the leading order of the real part and were originally considered by Federbush.³ We will study each diagram in a separate section, using the methods of Sec. II, and will sum them up in Sec. VII. We will explicitly study the backward Compton channel.

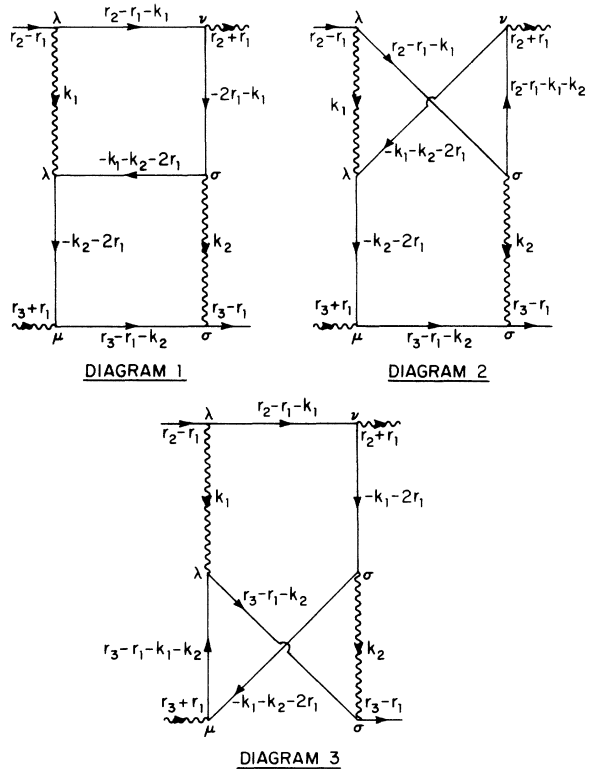


FIG. 4. The three sixth-order diagrams for Compton scattering near the backward direction that contribute to the leading order of the real part.

IV. FIRST SIXTH-ORDER DIAGRAM

The amplitude from diagram 1 of Fig. 4 is

$$\bar{\mathfrak{H}}_{1\mu\nu}^{(2)}(s, r_1) = g^6 \int d^4 k_1 (2\pi)^{-4} d^4 k_2 (2\pi)^{-4} [N_1^{(2)}]_{\mu\nu} D_1^{(2)-1}, \quad (4.1)$$

where

$$\begin{aligned} [N_1^{(2)}]_{\mu\nu} = & \bar{u}(r_3 - r_1) \gamma_\sigma (\not{r}_3 - \not{r}'_1 - \not{k}_2 + m) \gamma_\mu (-\not{k}_2 - 2\not{r}'_1 + m) \gamma_\lambda \\ & \times (-\not{k}_1 - \not{k}_2 - 2\not{r}'_1 + m) \gamma_\sigma (-2\not{r}'_1 - \not{k}_1 + m) \gamma_\nu (\not{r}'_2 - \not{r}'_1 - \not{k}_1 + m) \gamma_\lambda u(r_2 - r_1) \end{aligned} \quad (4.2)$$

and

$$\begin{aligned} D_1^{(2)} = & (k_1^2 - \lambda^2 + i\epsilon) [(r_2 - r_1 - k_1)^2 - m^2 + i\epsilon] [(2r_1 + k_1)^2 - m^2 + i\epsilon] \\ & \times [(k_1 + k_2 + 2r_1)^2 - m^2 + i\epsilon] [(k_2 + 2r_1)^2 - m^2 + i\epsilon] (k_2^2 - \lambda^2 + i\epsilon) [(r_3 - r_1 - k_2)^2 - m^2 + i\epsilon]. \end{aligned} \quad (4.3)$$

We first introduce $k_{1\pm}$ and $k_{2\pm}$ and approximate $D_1^{(2)}$ as

$$\begin{aligned} D_1^{(2)} \sim \bar{D}_1^{(2)} = & (k_{1+} k_{1-} - \bar{\mathbf{k}}_{1\perp}^2 - \lambda^2 + i\epsilon) [(k_{1+} - 2\omega) k_{1-} - (\bar{\mathbf{r}}_1 + \bar{\mathbf{k}}_{1\perp})^2 - m^2 + i\epsilon] \\ & \times [k_{1+} k_{1-} - (2\bar{\mathbf{r}}_1 + \bar{\mathbf{k}}_{1\perp})^2 - m^2 + i\epsilon] [(k_{1+} + k_{2+})(k_{1-} + k_{2-}) - (\bar{\mathbf{k}}_{1\perp} + \bar{\mathbf{k}}_{2\perp} + 2\bar{\mathbf{r}}_1)^2 - m^2 + i\epsilon] \\ & \times [k_{2+} k_{2-} - (\bar{\mathbf{k}}_{2\perp} + 2\bar{\mathbf{r}}_1)^2 - m^2 + i\epsilon] (k_{2+} k_{2-} - \bar{\mathbf{k}}_{2\perp}^2 - \lambda^2 + i\epsilon) [k_{2+} (k_{2-} - 2\omega) - (\bar{\mathbf{r}}_1 + \bar{\mathbf{k}}_{2\perp})^2 - m^2 + i\epsilon]. \end{aligned} \quad (4.4)$$

It may be verified that unless

$$0 < -k_{1-} < k_{2-} < 2\omega \quad (4.5)$$

the integration over either k_{1+} or k_{2+} (or both) gives zero. When (4.5) holds we may close the k_{2+} integration on the pole in the upper plane

$$k_{2+} = C_1 (k_{2-} - 2\omega)^{-1}, \quad (4.6a)$$

with

$$C_1 = (\bar{\mathbf{r}}_1 + \bar{\mathbf{k}}_{2\perp})^2 + m^2 - i\epsilon, \quad (4.6b)$$

and close the k_{1+} integration on the pole in the lower half plane

$$k_{1+} = -k_{2+} + C_2 (k_{1-} + k_{2-})^{-1}, \quad (4.7a)$$

with

$$C_2 = (\bar{\mathbf{k}}_{1\perp} + \bar{\mathbf{k}}_{2\perp} + 2\bar{\mathbf{r}}_1)^2 + m^2 - i\epsilon. \quad (4.7b)$$

Thus we obtain

$$\begin{aligned} \int d^4 k_1 d^4 k_2 \bar{D}_1^{(2)-1} = & -(\pi i)^2 \int d^2 \bar{\mathbf{k}}_{1\perp} d^2 \bar{\mathbf{k}}_{2\perp} \int_0^{2\omega} dk_{2-} \int_{-k_{2-}}^0 dk_{1-} (k_{2-} - 2\omega)^{-1} (k_{1-} + k_{2-})^{-1} \\ & \times \left[k_{1-} \left(\frac{C_1}{2\omega - k_{2-}} + \frac{C_2}{k_{1-} + k_{2-}} \right) - \bar{\mathbf{k}}_{1\perp}^2 - \lambda^2 + i\epsilon \right]^{-1} \\ & \times \left[-k_{1-} \left(2\omega - \frac{C_1}{2\omega - k_{2-}} - \frac{C_2}{k_{1-} + k_{2-}} \right) - (\bar{\mathbf{r}}_1 + \bar{\mathbf{k}}_{1\perp})^2 - m^2 + i\epsilon \right]^{-1} \\ & \times \left[k_{1-} \left(\frac{C_1}{2\omega - k_{2-}} + \frac{C_2}{k_{1-} + k_{2-}} \right) - (2\bar{\mathbf{r}}_1 + \bar{\mathbf{k}}_{1\perp})^2 - m^2 + i\epsilon \right]^{-1} \\ & \times \left[k_{2-} \left(\frac{C_1}{k_{2-} - 2\omega} \right) - (\bar{\mathbf{k}}_{2\perp} + 2\bar{\mathbf{r}}_1)^2 - m^2 + i\epsilon \right]^{-1} \\ & \times \left[k_{2-} \left(\frac{C_1}{k_{2-} - 2\omega} \right) - \bar{\mathbf{k}}_{2\perp}^2 - \lambda^2 + i\epsilon \right]^{-1}. \end{aligned} \quad (4.8)$$

The integration in the k_{1-}, k_{2-} plane is the triangle of Fig. 5. The largest contribution comes from the

boundaries of the triangle. More precisely, the reader may verify that the region with the largest contribution is

$$0 < -k_{1-} \ll k_{2-} \ll 2\omega. \quad (4.9)$$

In this region (4.8) is approximated by

$$\begin{aligned} & -(\pi i)^2 \int d^2\vec{k}_{1\perp} d^2\vec{k}_{2\perp} (-2\omega)^{-1} (-\vec{k}_{1\perp}^2 - \lambda^2)^{-1} [(2\vec{r}_1 + \vec{k}_{1\perp})^2 - m^2]^{-1} [(\vec{k}_{2\perp} + 2\vec{r}_1)^2 - m^2]^{-1} (-\vec{k}_{2\perp}^2 - \lambda^2)^{-1} \\ & \times \int_0^{2\omega} dk_{2-} \int_{-k_{2-}}^0 dk_{1-} k_{2-}^{-1} [-2\omega k_{1-} - (\vec{r}_1 + \vec{k}_{1\perp})^2 - m^2 + i\epsilon]^{-1} \\ & \doteq (\pi i)^2 (2\omega)^{-2\frac{1}{2}} [\ln^2 s - 2\pi i \ln s] \\ & \times \int d^2\vec{k}_{1\perp} d^2\vec{k}_{2\perp} (\vec{k}_{1\perp}^2 + \lambda^2)^{-1} [(2\vec{r}_1 + \vec{k}_{1\perp})^2 + m^2]^{-1} [(2\vec{r}_1 + \vec{k}_{2\perp})^2 + m^2]^{-1} (\vec{k}_{2\perp}^2 + \lambda^2)^{-1}. \quad (4.10) \end{aligned}$$

We now turn to the approximation of the numerator (4.2). Again, because both the k_+ poles of (4.6) and (4.7) and the k_- region (4.9) are small compared with 2ω we neglect k_1 and k_2 when they are compared with r_2 or r_3 . Therefore

$$[N_1^{(2)}]_{\mu\nu} \sim 4\bar{u}(r_3 - r_1)\gamma_\mu (-\not{k}_2 - 2\not{r}_1 + m)\not{r}_2 (-\not{k}_1 - \not{k}_2 - 2\not{r}_1 + m)\not{r}_3 (-2\not{r}_1 - \not{k}_1 + m)\gamma_\nu u(r_2 - r_1). \quad (4.11)$$

Now, to leading order (recalling that μ and ν take on only the values x and y)

$$\bar{u}(r_3 - r_1)\gamma_\mu (-\not{k}_2 - 2\not{r}_1 + m)\not{r}_2 \sim \bar{u}(r_3 - r_1)\gamma_\mu (-\vec{k}_{2\perp} - 2\vec{r}_{1\perp} + m)\not{r}_2, \quad (4.12a)$$

$$\not{r}_3 (-2\not{r}_1 - \not{k}_1 + m)\gamma_\nu u(r_2 - r_1) \sim \not{r}_3 (-2\vec{r}_{1\perp} - \vec{k}_{1\perp} + m)\gamma_\nu u(r_2 - r_1), \quad (4.12b)$$

and

$$\not{r}_2 (-\not{k}_1 - \not{k}_2 - 2\not{r}_1 + m)\not{r}_3 \sim \not{r}_2 (-\vec{k}_{1\perp} - \vec{k}_{2\perp} - 2\vec{r}_{1\perp} + m)\not{r}_3, \quad (4.12c)$$

where we have used the Dirac equation (2.18) and

$$(\gamma_0 + \gamma_3)^2 = 0. \quad (4.13)$$

Using (4.12) in (4.11) and anticommuting \not{r}_3 to the left we find to leading order

$$[N_1^{(2)}]_{\mu\nu} \sim 8(r_2 \cdot r_3) \bar{u}(r_3 - r_1)\gamma_\mu (-\vec{k}_{2\perp} - 2\vec{r}_{1\perp} + m)(\vec{k}_{1\perp} + \vec{k}_{2\perp} + 2\vec{r}_{1\perp} + m)(-\vec{k}_{1\perp} - 2\vec{r}_{1\perp} + m)\gamma_\nu u(r_2 - r_1). \quad (4.14)$$

This does not depend on k_{1-} or k_{2-} . Therefore, we may insert it into (4.10) to find

$$\begin{aligned} \bar{\mathfrak{N}}_{\mu\nu}^{(2)}(s, r_1) & \doteq -g^6 \frac{1}{2} [\ln^2 s - 2\pi i \ln s] \int d^2\vec{k}_{1\perp} (2\pi)^{-3} d^2\vec{k}_{2\perp} (2\pi)^{-3} \\ & \times (\vec{k}_{1\perp}^2 + \lambda^2)^{-1} [(2\vec{r}_1 + \vec{k}_{1\perp})^2 + m^2]^{-1} [(2\vec{r}_1 + \vec{k}_{2\perp})^2 + m^2]^{-1} (\vec{k}_{2\perp}^2 + \lambda^2)^{-1} \\ & \times \bar{u}(r_3 - r_1)\gamma_\mu (-\vec{k}_{2\perp} - 2\vec{r}_{1\perp} + m)(\vec{k}_{1\perp} + \vec{k}_{2\perp} + 2\vec{r}_{1\perp} + m)(-\vec{k}_{1\perp} - 2\vec{r}_{1\perp} + m)\gamma_\nu u(r_2 - r_1). \quad (4.15) \end{aligned}$$

V. SECOND SIXTH-ORDER DIAGRAM

Consider next diagram 2 of Fig. 3. Its Feynman amplitude is

$$\bar{\mathfrak{N}}_{2\mu\nu}^{(2)}(s, r_1) = g^6 \int d^4k_1 (2\pi)^{-4} d^4k_2 (2\pi)^{-4} [N_2^{(2)}]_{\mu\nu} D_2^{(2)-1}, \quad (5.1)$$

where

$$\begin{aligned} [N_2^{(2)}]_{\mu\nu} & = \bar{u}(r_3 - r_1)\gamma_\sigma (\not{r}_3 - \not{k}_2 - \not{r}_1 + m)\gamma_\mu (-\not{k}_2 - 2\not{r}_1 + m)\gamma_\lambda \\ & \times (-\not{k}_1 - \not{k}_2 - 2\not{r}_1 + m)\gamma_\nu (\not{r}_2 - \not{r}_1 - \not{k}_1 - \not{k}_2 + m)\gamma_\sigma (\not{r}_2 - \not{r}_1 - \not{k}_1 + m)\gamma_\lambda u(r_2 - r_1) \quad (5.2) \end{aligned}$$

and

$$D_2^{(2)} = (k_1^2 - \lambda^2 + i\epsilon)[(r_2 - r_1 - k_1)^2 - m^2 + i\epsilon][(r_2 - r_1 - k_1 - k_2)^2 - m^2 + i\epsilon] \\ \times [(k_1 + k_2 + 2r_1)^2 - m^2 + i\epsilon][(k_2 + 2r_1)^2 - m^2 + i\epsilon][k_2^2 - \lambda^2 + i\epsilon][(r_3 - r_1 - k_2)^2 - m^2 + i\epsilon]. \quad (5.3)$$

We first introduce the coordinates $k_{1\pm}$ and $k_{2\pm}$ and make the usual approximation $r_{1\pm} = r_{2\pm} = r_{3\pm} = 0$ to find

$$D_2^{(2)} \sim \bar{D}_2^{(2)} = (k_{1+}k_{1-} - \vec{k}_{1\perp}^2 - \lambda^2 + i\epsilon)(k_{1+} - 2\omega)k_{1-} - (\vec{k}_{1\perp} + \vec{r}_\perp)^2 - m^2 + i\epsilon \\ \times [(k_{1+} + k_{2+} - 2\omega)(k_{1-} + k_{2-}) - (\vec{k}_{1\perp} + \vec{k}_{2\perp} + \vec{r}_\perp)^2 - m^2 + i\epsilon] \\ \times [(k_{1+} + k_{2+})(k_{1-} + k_{2-}) - (\vec{k}_{1\perp} + \vec{k}_{2\perp} + 2\vec{r}_\perp)^2 - m^2 + i\epsilon] \\ \times [k_{2+}k_{2-} - (\vec{k}_{2\perp} + 2\vec{r}_\perp)^2 - m^2 + i\epsilon](k_{2+}k_{2-} - \vec{k}_{2\perp}^2 - \lambda^2 + i\epsilon)[k_{2+}(k_{2-} - 2\omega) - (\vec{k}_{2\perp} + \vec{r}_\perp)^2 - m^2 + i\epsilon]. \quad (5.4)$$

Again it may be verified that if we integrate over k_{1+} and k_{2+} the integral vanishes unless (4.5) holds. When (4.5) does hold we close the k_{2+} integration at the pole in the upper half plane,

$$k_{2+} = C_1(k_{2-} - 2\omega)^{-1}, \quad (5.5a)$$

with

$$C_1 = (\vec{k}_{2\perp} + \vec{r}_\perp)^2 + m^2 - i\epsilon, \quad (5.5b)$$

and close the k_{1+} integration on the two poles in the lower half plane,

$$k_{1+} = -k_{2+} + C_2(k_{1-} + k_{2-})^{-1}, \quad (5.6a)$$

with

$$C_2 = (\vec{k}_{1\perp} + \vec{k}_{2\perp} + 2\vec{r}_\perp)^2 + m^2 - i\epsilon, \quad (5.6b)$$

and

$$k_{1+} = 2\omega - k_{2+} + C_3(k_{1-} + k_{2-})^{-1}, \quad (5.7a)$$

with

$$C_3 = (\vec{k}_{1\perp} + \vec{k}_{2\perp} + \vec{r}_\perp)^2 + m^2 - i\epsilon. \quad (5.7b)$$

(For convenience we redefine the symbols C_i in each section where they are used and in general the C_i of one section will not be equal to the C_i of any other section.)

We now turn to the approximation of the numerator. Because of (5.7) we cannot always neglect $k_{1+} + k_{2+}$ when compared with r_2 . We will also keep k_{2-} when compared with r_3 . Therefore, in (5.2) we drop k_{2+} in the first factor and k_{1-} and k_{2-} in the last two factors. We then anticommute $\gamma_3 - \not{k}_{2-}$ to the left, anticommute $\gamma_2 - \not{k}_{1+}$ to the right, and use the Dirac equation to obtain

$$[N_2^{(2)}]_{\mu\nu} \sim 4\bar{u}(r_3 - r_1)\gamma_\mu(-\not{k}_2 - 2\not{\gamma}_1 + m)(\not{\gamma}_2 - \not{k}_{1+}) \\ \times (-\not{k}_1 - \not{k}_2 - 2\not{\gamma}_1 + m)\gamma_\nu(\not{\gamma}_2 - \not{k}_{1+} - \not{k}_{2+}) \\ \times (\not{\gamma}_3 - \not{k}_{2-})u(r_2 - r_1). \quad (5.8)$$

Then anticommute $\not{\gamma}_2 - \not{k}_{1+} - \not{k}_{2+}$ to the right and obtain

$$[N_2^{(2)}]_{\mu\nu} \sim 4(2\omega - k_{1+} - k_{2+})(2\omega - k_{2-})\bar{u}(r_3 - r_1) \\ \times \gamma_\mu(-\not{k}_2 - 2\not{\gamma}_1 + m)(\not{\gamma}_2 - \not{k}_{1+}) \\ \times (-\not{k}_1 - \not{k}_2 - 2\not{\gamma}_1 + m)\gamma_\nu u(r_2 - r_1). \quad (5.9)$$

Since μ and ν are restricted to x and y we may further approximate

$$\bar{u}(r_3 - r_1)\gamma_\mu(-\not{k}_2 - 2\not{\gamma}_1 + m)(\not{\gamma}_2 - \not{k}_{1+}) \\ \sim \bar{u}(r_3 - r_1)\gamma_\mu(-\vec{k}_{2\perp} - 2\vec{r}_\perp + m)(\not{\gamma}_2 - \not{k}_{1+}) \quad (5.10)$$

and anticommute $\not{\gamma}_2 - \not{k}_{1+}$ to the right to find

$$[N_2^{(2)}]_{\mu\nu} \sim -4(2\omega - k_{1+} - k_{2+})(2\omega - k_{2-})(2\omega - k_{1+}) \\ \times (k_{1-} + k_{2-})\bar{u}(r_3 + r_1)\gamma_\mu(-\vec{k}_{2\perp} - 2\vec{r}_\perp + m) \\ \times \gamma_\nu u(r_2 - r_1). \quad (5.11)$$

We now use this numerator with the approximated denominator of (5.4). It may be verified that the factor $2\omega - k_{1+} - k_{2+}$ in (5.11) suppresses the contribution from the k_{1+} pole (5.7). Therefore, we need only consider the k_{1+} pole (5.6) and we find

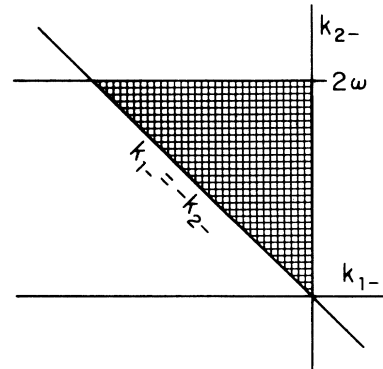


FIG. 5. The integration region in the (k_{1-}, k_{2-}) plane for the sixth-order Feynman diagrams 1 and 2.

$$\begin{aligned}
\bar{\mathfrak{M}}_{2\mu\nu}^{(2)}(s, r_1) &\doteq g^6 (2\pi i)^2 \int d^2\bar{\mathbf{k}}_{1\perp} (2\pi)^{-4} \int d^2\bar{\mathbf{k}}_{2\perp} (2\pi)^{-4} (-s) \bar{u}(r_3 - r_1) \gamma_\mu (-\bar{\mathbf{k}}_{2\perp} - 2\bar{\mathbf{r}}_{1\perp} + m) \gamma_\nu u(r_2 - r_1) \\
&\times \int_0^{2\omega} dk_{2-} \int_{-k_{2-}}^0 dk_{1-} [k_{2-} C_1 (2\omega - k_{2-})^{-1} - \bar{\mathbf{k}}_{2\perp}^2 - \lambda^2 + i\epsilon]^{-1} \\
&\times [k_{2-} C_2 (2\omega - k_{2-})^{-1} - (\bar{\mathbf{k}}_{2\perp} + 2\bar{\mathbf{r}}_{1\perp})^2 - m^2 + i\epsilon]^{-1} \\
&\times \{k_{1-} [-C_1 (2\omega - k_{2-})^{-1} + C_2 (k_{1-} + k_{2-})^{-1}] - \bar{\mathbf{k}}_{1\perp}^2 - \lambda^2 + i\epsilon\}^{-1} \\
&\times \{k_{1-} [-2\omega - C_1 (2\omega - k_{2-})^{-1} + C_2 (k_{1-} + k_{2-})^{-1}] - (\bar{\mathbf{k}}_{1\perp} + \bar{\mathbf{r}}_{1\perp})^2 - m^2 + i\epsilon\}^{-1} \\
&\times \{(k_{1-} + k_{2-}) [-2\omega + C_2 (k_{1-} + k_{2-})^{-1}] - (\bar{\mathbf{k}}_{1\perp} + \bar{\mathbf{k}}_{2\perp} + \bar{\mathbf{r}}_{1\perp})^2 - m^2 + i\epsilon\}^{-1}, \quad (5.12)
\end{aligned}$$

which may be further approximated as

$$\begin{aligned}
\bar{\mathfrak{M}}_{2\mu\nu}^{(2)}(s, r_1) &\doteq -g^6 s \int d^2\bar{\mathbf{k}}_{1\perp} (2\pi)^{-3} d^2\bar{\mathbf{k}}_{2\perp} (2\pi)^{-3} \bar{u}(r_3 - r_1) \gamma_\mu (-\bar{\mathbf{k}}_{2\perp} - 2\bar{\mathbf{r}}_{1\perp} + m) \gamma_\nu u(r_2 - r_1) (\bar{\mathbf{k}}_{2\perp}^2 + \lambda^2)^{-1} [(\bar{\mathbf{k}}_{2\perp} + 2\bar{\mathbf{r}}_{1\perp})^2 + m^2]^{-1} \\
&\times \int_0^{2\omega} dk_{2-} \int_{-k_{2-}}^0 dk_{1-} [k_{1-} C_2 (k_{1-} + k_{2-})^{-1} - \bar{\mathbf{k}}_{1\perp}^2 - \lambda^2 + i\epsilon]^{-1} [-2\omega k_{1-} - (\bar{\mathbf{k}}_{1\perp} + \bar{\mathbf{r}}_{1\perp})^2 - m^2 + i\epsilon]^{-1} \\
&\times [-2\omega (k_{1-} + k_{2-}) - (\bar{\mathbf{k}}_{1\perp} + \bar{\mathbf{k}}_{2\perp} + \bar{\mathbf{r}}_{1\perp})^2 - m^2 + C_2 + i\epsilon]^{-1}. \quad (5.13)
\end{aligned}$$

The integration region is again the triangular region of Fig. 5 and it may be seen that the largest contribution comes from the region

$$0 < -k_{1-} \ll k_{2-} \ll 2\omega. \quad (5.14)$$

Thus (5.13) reduces to

$$\begin{aligned}
\bar{\mathfrak{M}}_{2\mu\nu}^{(2)}(s, r_1) &\doteq g^6 s \int d^2\bar{\mathbf{k}}_{1\perp} (2\pi)^{-3} d^2\bar{\mathbf{k}}_{2\perp} (2\pi)^{-3} \bar{u}(r_3 - r_1) \gamma_\mu (-\bar{\mathbf{k}}_{2\perp} - 2\bar{\mathbf{r}}_{1\perp} + m) \gamma_\nu u(r_2 - r_1) \\
&\times (\bar{\mathbf{k}}_{1\perp}^2 + \lambda^2)^{-1} (\bar{\mathbf{k}}_{2\perp}^2 + \lambda^2)^{-1} [(\bar{\mathbf{k}}_{2\perp} + 2\bar{\mathbf{r}}_{1\perp})^2 + m^2]^{-1} \\
&\times \int_0^{2\omega} dk_{2-} [2\omega k_{2-} + (\bar{\mathbf{k}}_{1\perp} + \bar{\mathbf{k}}_{2\perp} + \bar{\mathbf{r}}_{1\perp})^2 - (\bar{\mathbf{k}}_{1\perp} + \bar{\mathbf{k}}_{2\perp} + 2\bar{\mathbf{r}}_{1\perp})^2]^{-1} \\
&\times \int_{-k_{2-}}^0 dk_{1-} [-2\omega k_{1-} - (\bar{\mathbf{k}}_{1\perp} + \bar{\mathbf{r}}_{1\perp})^2 - m^2 + i\epsilon]^{-1}. \quad (5.15)
\end{aligned}$$

The smallest integration variable is k_{1-} and, as $\epsilon \rightarrow 0$, there is a pole on the integration path of k_{1-} . This pole gives rise to an imaginary part of order $\ln s$. There may also be a pole on the integration path of the next smallest integration variable (k_{2-} in this case). Such a pole can only give rise to an imaginary part of $O(1)$. Indeed, it is a general feature of the integrals we are considering over regions like (5.14) that if in n th order the real part is of order $\ln^n s$, then an imaginary part of order $\ln^{n-1} s$ can only come from a pole on the integration path of the smallest variable of integration.

With this remark we find the desired result

$$\begin{aligned}
\bar{\mathfrak{M}}_{2\mu\nu}^{(2)}(s, r_1) &\doteq g^6 \frac{1}{2} (\ln^2 s - 2\pi i \ln s) \int d^2\bar{\mathbf{k}}_{1\perp} d^2\bar{\mathbf{k}}_{2\perp} \bar{u}(r_3 - r_1) \gamma_\mu (-\bar{\mathbf{k}}_{2\perp} - 2\bar{\mathbf{r}}_{1\perp} + m) \gamma_\nu u(r_2 - r_1) \\
&\times (\bar{\mathbf{k}}_{1\perp}^2 + \lambda^2)^{-1} (\bar{\mathbf{k}}_{2\perp}^2 + \lambda^2)^{-1} [(\bar{\mathbf{k}}_{2\perp} + 2\bar{\mathbf{r}}_{1\perp})^2 + m^2]^{-1}. \quad (5.16)
\end{aligned}$$

VI. THIRD SIXTH-ORDER DIAGRAM

The amplitude for diagram 3 of Fig. 4 may be obtained from that of diagram 2 by the replacements $k_1 \rightarrow k_2$, $\mu \leftrightarrow \nu$ and by inverting the order of all γ matrices. Therefore

$$\begin{aligned}
\bar{\mathfrak{M}}_{3\mu\nu}^{(2)}(s, r_1) &\doteq g^6 \frac{1}{2} (\ln^2 s - 2\pi i \ln s) \int d^2\bar{\mathbf{k}}_{1\perp} (2\pi)^{-3} d^2\bar{\mathbf{k}}_{2\perp} (2\pi)^{-3} \bar{u}(r_3 - r_1) \gamma_\mu (-\bar{\mathbf{k}}_{1\perp} - 2\bar{\mathbf{r}}_{1\perp} + m) \gamma_\nu u(r_2 - r_1) \\
&\times (\bar{\mathbf{k}}_{1\perp}^2 + \lambda^2)^{-1} (\bar{\mathbf{k}}_{2\perp}^2 + \lambda^2)^{-1} [(2\bar{\mathbf{r}}_{1\perp} + \bar{\mathbf{k}}_{1\perp})^2 + m^2]^{-1}. \quad (6.1)
\end{aligned}$$

VII. SUMMATION OF DIAGRAMS 1, 2, AND 3

The separate expressions (4.15), (5.16), and (6.1) do not converge when the cutoff in the transverse-momentum integrations is removed. Therefore, for our evaluations to make sense these logarithmic divergences in the separate integrals must cancel.

To see that this cancellation does in fact occur, we first rewrite (4.15) using

$$\begin{aligned}
& (-\vec{k}_{2\perp} - 2\vec{f}_{\perp} + m)(\vec{k}_{1\perp} + \vec{k}_{2\perp} + 2\vec{f}_{\perp} + m)(-\vec{k}_{1\perp} - 2\vec{f}_{\perp} + m) \\
&= (-\vec{k}_{2\perp} - 2\vec{f}_{\perp} + m)[(\vec{k}_{2\perp} + 2\vec{f}_{\perp} + m) + (\vec{k}_{1\perp} + 2\vec{f}_{\perp} + m) - (2\vec{f}_{\perp} + m)](-\vec{k}_{1\perp} - 2\vec{f}_{\perp} + m) \\
&= [(\vec{k}_{2\perp} + 2\vec{f}_{\perp})^2 + m^2](-\vec{k}_{1\perp} - 2\vec{f}_{\perp} + m) + [(\vec{k}_{1\perp} + 2\vec{f}_{\perp})^2 + m^2](-\vec{k}_{2\perp} - 2\vec{f}_{\perp} + m) - (\vec{k}_{2\perp} + 2\vec{f}_{\perp} - m)(2\vec{f}_{\perp} + m)(\vec{k}_{1\perp} + 2\vec{f}_{\perp} - m).
\end{aligned} \tag{7.1}$$

The terms in $\tilde{\mathfrak{N}}_{1\mu\nu}^{(2)}(s, r_1)$ which correspond to the first two terms in (7.1) cancel (5.16) and (6.1). Therefore we obtain the desired result

$$\begin{aligned}
& \tilde{\mathfrak{N}}_{1\mu\nu}^{(2)}(s, r_1) + \tilde{\mathfrak{N}}_{2\mu\nu}^{(2)}(s, r_1) + \tilde{\mathfrak{N}}_{3\mu\nu}^{(2)}(s, r_1) \\
& \doteq g^{\frac{6}{2}}(\ln^2 s - 2\pi i \ln s) \\
& \quad \times \int d^2 \vec{k}_{1\perp} (2\pi)^{-3} d^2 \vec{k}_{2\perp} (2\pi)^{-3} \bar{u}(r_3 - r_1) \gamma_{\mu} (\vec{k}_{2\perp} + 2\vec{f}_{\perp} - m)(2\vec{f}_{\perp} + m)(\vec{k}_{1\perp} + 2\vec{f}_{\perp} - m) \gamma_{\nu} u(r_2 - r_1) \\
& \quad \times (\vec{k}_{1\perp}^2 + \lambda^2)^{-1} [(\vec{k}_{1\perp} + 2\vec{f}_{\perp})^2 + m^2]^{-1} (\vec{k}_{2\perp}^2 + \lambda^2)^{-1} [(\vec{k}_{2\perp} + 2\vec{f}_{\perp})^2 + m^2]^{-1} \\
& \doteq g^{\frac{2}{2}}(\ln^2 s - 2\pi i \ln s) \bar{u}(r_3 - r_1) \gamma_{\mu} \frac{1}{2\vec{f}_{\perp} + m} [\alpha(2\vec{f}_{\perp})]_{\nu} \gamma_{\nu} u(r_2 - r_1).
\end{aligned} \tag{7.2}$$

Here the cutoff may be removed as all the logarithmic divergences have cancelled. This result (7.2) is the same as that previously obtained using Feynman parameters.¹

VIII. MOMENTUM-FLOW DIAGRAMS

In the evaluation of the leading asymptotic behavior of Feynman integrals by means of the momentum-space techniques used above it is always necessary to answer two questions: (1) What region in minus-momentum space gives a nonzero contribution after the plus-momentum integrations have been done? (2) Which poles should the plus-momentum integration contours be closed on? For the three sixth-order diagrams already considered, the answers to these two questions posed no big problem. However, for more complicated diagrams of higher order it can become very tedious to answer these questions algebraically. Therefore we will introduce a diagrammatic technique to find the answers to these questions.

To each Feynman diagram there correspond, in general, several "momentum flow" diagrams. These diagrams consist of arrows drawn on the Feynman diagram. The arrows represent the direction of flow of the minus component of momenta in that line (i.e., the direction such that if q , the momentum of that line, points in that direction, then $q_0 - q_3 > 0$). The arrows are drawn according to the following rules:

1. At least one arrow must point towards and one arrow must point away from each vertex that does not connect to an external line. (This is the conservation of minus momentum, which follows from the conservation of four momenta at each vertex.)
2. If an external line carries no minus momentum when $\omega \rightarrow \infty$ (such as $r_{2\pm} r_1$), then on the two internal lines that connect to it one arrow must point towards the vertex and the other arrow must point away from the vertex.
3. The incoming line that carries the momentum r_3 acts as a source of minus momenta and the arrows on the two internal lines connecting to it point away from the vertex.
4. The outgoing line that carries the momentum r_3 acts as a sink of minus momentum and the arrows on the two internal lines connecting to it point towards the vertex.
5. There must be no closed loops in which *all* arrows point in the same direction around the loop. These rules determine the contributing regions in the space of minus momentum.

The first four rules follow from momentum conservation. The fifth rule follows from the following consideration. There are several different ways to introduce momentum coordinates into a Feynman diagram. If there is a closed loop around which the arrows all point in the same direction, choose one of the momentum coordinates (say q) to flow around that loop in the direction of

the arrow. The integral over q_+ will then consist of an integral with many factors of the form $(p_{l+}p_{l-} - \vec{p}_{l\perp}^2 - m_l^2 + i\epsilon)^{-1}$, where there is one such factor for each line in the closed loop, the four-vector p_l is the momentum in the l th line, and m_l is the mass of the line. By construction all the $p_{l-} > 0$ and each p_{l+} is of the form q_+ + something. Therefore, all the poles of this q_+ integration are in the lower half plane and the integration gives zero. Therefore rule 5 follows.

Now suppose that in this loop not all arrows point in the same direction. Then if we let the loop momentum q flow in one direction around the loop, an argument similar to the one just given shows that we may close the contour of the q_+ integration on the poles represented either by the arrows that point in the direction of q or that oppose the direction of q . When we close on a particular pole which contains the momentum p_l this argument shows that we obtain

$$-2\pi i |p_{l-}|^{-1} \times [\text{the rest of the integral with } p_{l+} = p_{l-}^{-1}(\vec{p}_{l\perp}^2 + m_l^2)]. \quad (8.1)$$

From this discussion we see that we may determine which poles to close on by drawing the independent loops which we integrate over. Different loops may be used with each of the (in general) several momentum-flow diagrams associated with a given Feynman diagram. We would like to indi-

cate these loops by drawing them on the momentum-flow diagrams. Unfortunately, in a black and white drawing this is almost impossible to do because the loops cross so many times. Therefore, we have labeled all vertices of our momentum flow diagrams by letters and in the captions give the letters of the vertices that make up each integration loop. The reader is urged to trace out these loops with colored pencils.

Once the integration loops are chosen it is easy to read off the contributing poles. These poles are marked by crosses on our diagrams. The number by each cross indicates which loop momenta is closed upon the pole.

To illustrate these rules we consider the three sixth-order diagrams already studied. In Fig. 6 we give the one momentum-flow diagram associated with the first sixth-order Feynman diagram of Fig. 4. Using the coordinates of Fig. 4 with the arrows of Fig. 6 we have

$$k_{1-} < 0, \quad (8.2a)$$

$$k_{2-} > 0, \quad (8.2b)$$

$$k_{1-} + k_{2-} > 0, \quad (8.2c)$$

and

$$2\omega - k_{2-} > 0. \quad (8.2d)$$

Restriction (8.2b) is not independent of (8.2a) and (8.2c). The remaining three restrictions are just the inequalities (4.5).

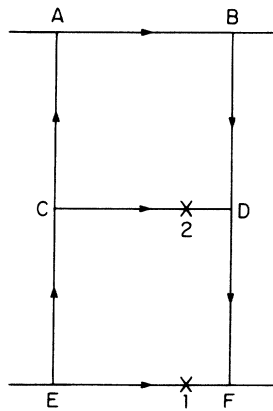


DIAGRAM 1

FIG. 6. Momentum-flow diagram for the sixth-order Feynman diagram 1. The first plus-(+) momentum integral is over the momentum in the loop $ECDFE$. The second integral is over the momentum in the loop $CABDC$. The poles closed on in doing these integrals are indicated by crosses.

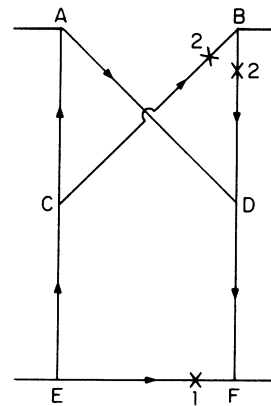


DIAGRAM 2

FIG. 7. Momentum-flow diagram for the sixth-order Feynman diagram 2. The first momentum loop is $BDFECD$. The second momentum loop is $ADBCA$. The poles closed on are indicated by crosses.

The two momentum loops in Fig. 6 we choose to integrate over are $ECDFE$ and $CABDC$. We may then close on the poles indicated on the diagram. This gives the poles (4.6) and (4.7).

Finally, use of the formula (8.1) gives (4.8)

The momentum-flow diagram for the second sixth-order diagram of Fig. 4 is given in Fig. 7. The reader should convince himself that the arrows give the momentum region (4.5) and that the poles determined from the indicated loops give (5.5), (5.6), and (5.7).

In Fig. 8 we show the two momentum-flow diagrams corresponding to the third sixth-order diagram of Fig. 4. However, these diagrams never have to be used since Feynman diagram 3 may be obtained from Feynman diagram 2 as discussed in Sec. VI.

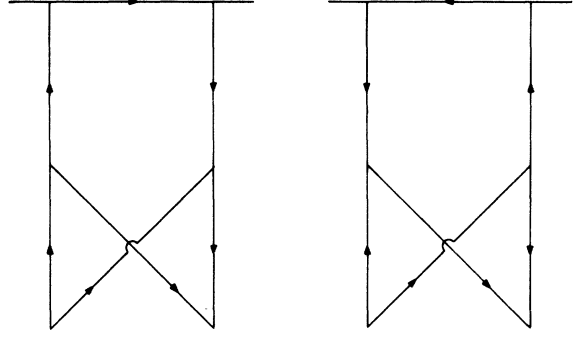


FIG. 8. The two momentum-flow diagrams for the sixth-order Feynman diagram 3.

IX. SIXTH-ORDER DIAGRAMS THAT CONTRIBUTE TO THE LEADING IMAGINARY PART

There are no diagrams other than those of Fig. 4 which (when the integrals over transverse momentum are cut off at k_{\max}) have a real part of order $\ln^2 s$. Furthermore, the sum of the three diagrams of Fig. 4 has an imaginary part of order $\ln s$ which is given in (7.2). However, if we want the *complete* coefficient of order $\ln s$ of the imaginary part of the sixth-order amplitude, we must also include diagram 4 given in Fig. 9 which corresponds to the following amplitude:

$$\bar{\mathfrak{M}}_{4\mu\nu}^{(2)}(s, r_1) = g^6 \int d^4 k_1 (2\pi)^{-4} d^4 k_2 (2\pi)^{-4} [N_4^{(2)}]_{\mu\nu} D_4^{(2)-1}, \quad (9.1)$$

where

$$\begin{aligned} [N_4^{(2)}]_{\mu\nu} = & \bar{u}(r_3 - r_1) \gamma_\sigma (\not{r}_3 - \not{r}_1 - \not{k}_2 + m) \gamma_\lambda (\not{r}_3 - \not{r}_1 - \not{k}_1 - \not{k}_2 + m) \gamma_\mu (-\not{k}_1 - \not{k}_2 - 2\not{r}_1 + m) \gamma_\nu \\ & \times (\not{r}_2 - \not{r}_1 - \not{k}_1 - \not{k}_2 + m) \gamma_\sigma (\not{r}_2 - \not{r}_1 - \not{k}_1 + m) \gamma_\lambda u(r_2 - r_1) \end{aligned} \quad (9.2)$$

and

$$\begin{aligned} D_4^{(2)} = & (k_1^2 - \lambda^2 + i\epsilon) [(r_2 - r_1 - k_1)^2 - m^2 + i\epsilon] [(r_2 - r_1 - k_1 - k_2)^2 - m^2 + i\epsilon] \\ & \times [(k_1 + k_2 + 2r_1)^2 - m^2 + i\epsilon] [(r_3 - r_1 - k_1 - k_2)^2 - m^2 + i\epsilon] [(r_3 - r_1 - k_2)^2 - m^2 + i\epsilon] (k_2^2 - \lambda^2 + i\epsilon). \end{aligned} \quad (9.3)$$

The numerator is easily approximated by first replacing $\not{r}_3 - \not{r}_1 - \not{k}_1 + m$ with $\not{r}_3 - \not{k}_{1-}$, replacing $\not{r}_3 - \not{r}_1 - \not{k}_1 - \not{k}_2 + m$ with $\not{r}_3 - \not{k}_{1-} - \not{k}_{2-}$, replacing $\not{r}_2 - \not{r}_1 - \not{k}_1 - \not{k}_2 + m$ with $\not{r}_2 - \not{k}_{1+} - \not{k}_{2+}$, and replacing $\not{r}_2 - \not{r}_1 - \not{k}_1 + m$ with $\not{r}_2 - \not{k}_{1+}$. Then we find

$$\begin{aligned} [N_4^{(2)}]_{\mu\nu} \sim & 4(2\omega - k_{2-})(2\omega - k_{1+} - k_{2+})(2\omega - k_{1-} - k_{2-}) \\ & \times (2\omega - k_{1+}) \bar{u}(r_3 - r_1) \gamma_\mu (-\vec{k}_{1\perp} - \vec{k}_{2\perp} - 2\vec{r}_{1\perp} + m) \gamma_\nu u(r_2 - r_1). \end{aligned} \quad (9.4)$$

Furthermore, using $k_{1\pm}$ and $k_{2\pm}$ as variables and using the approximation $r_{2-} = r_{3+} = r_{1\pm} = 0$ the denominator $D_4^{(2)}$ is approximated as

$$\begin{aligned} D_4^{(2)} \sim \bar{D}_4^{(2)} = & (k_{1+} k_{1-} - \vec{k}_{1\perp}^2 - \lambda^2 + i\epsilon) [(k_{1+} - 2\omega) k_{1-} - (\vec{k}_{1\perp} + \vec{r}_{1\perp})^2 - m^2 + i\epsilon] \\ & \times [(k_{1+} + k_{2+} - 2\omega)(k_{1-} + k_{2-}) - (\vec{k}_{1\perp} + \vec{k}_{2\perp} + \vec{r}_{1\perp})^2 - m^2 + i\epsilon] \\ & \times [(k_{1+} + k_{2+})(k_{1-} + k_{2-}) - (\vec{k}_{1\perp} + \vec{k}_{2\perp} + 2\vec{r}_{1\perp})^2 - m^2 + i\epsilon] \\ & \times [(k_{1+} + k_{2+})(k_{1-} + k_{2-} - 2\omega) - (\vec{k}_{2\perp} + \vec{r}_{1\perp})^2 - m^2 + i\epsilon] \\ & \times [k_{2+}(k_{2-} - 2\omega) - (\vec{k}_{2\perp} + \vec{r}_{1\perp})^2 - m^2 + i\epsilon] (k_{2+} k_{2-} - \vec{k}_{2\perp}^2 - \lambda^2 + i\epsilon) \end{aligned} \quad (9.5)$$

There are two momentum-flow diagrams for this one Feynman diagram (Fig. 10). We consider them separately.

A. Diagram A

We find from Fig. 10 that for diagram A the momentum region is

$$\begin{aligned} 0 < k_{2-} < 2\omega, \\ 0 < k_{1-} + k_{2-} < 2\omega, \\ k_{1-} < 0 \end{aligned} \quad (9.6)$$

(see Fig. 11), and the poles are

$$k_{2+} = C_1(2\omega - k_{2-})^{-1} \quad (9.7a)$$

and

$$k_{1+} = \begin{cases} -k_{2+} + C_2(k_{1-} + k_{2-})^{-1} \\ 2\omega - k_{2+} + C_3(k_{1-} + k_{2-})^{-1}, \end{cases} \quad (9.7b)$$

$$(9.7b')$$

where

$$C_1 = (\vec{k}_{2\perp} + \vec{r}_\perp)^2 + m^2 - i\epsilon, \quad (9.8a)$$

$$C_2 = (\vec{k}_{1\perp} + \vec{k}_{2\perp} + 2\vec{r}_\perp)^2 + m^2 - i\epsilon, \quad (9.8b)$$

and

$$C_3 = (\vec{k}_{1\perp} + \vec{k}_{2\perp} + \vec{r}_\perp)^2 + m^2 - i\epsilon, \quad (9.8c)$$

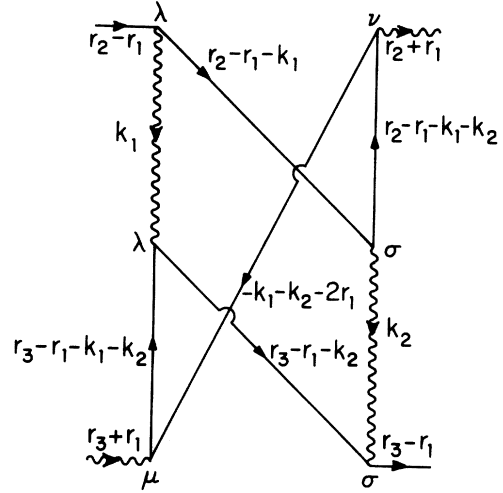


FIG. 9. A sixth-order Feynman diagram for Compton scattering in the backward direction which has an imaginary part of the order $\ln s$. This diagram is called 4. This diagram must be included with those of Fig. 4 to obtain the complete leading contribution to the imaginary part of the sixth-order backward Compton amplitude.

The factor $2\omega - k_{1+} - k_{2+}$ in the numerator (9.4) suppresses contribution from the pole (9.7b'). Therefore only (9.7b) contributes and we find that the contribution from diagram A, called \mathcal{G}_A , is

$$\begin{aligned} \mathcal{G}_A \doteq & -g^6(2\pi i)^2 \int d^2\vec{k}_{1\perp} (2\pi)^{-4} d^2\vec{k}_{2\perp} (2\pi)^{-4} (2\omega)^3 \bar{u}(r_3 - r_1) \gamma_\mu (-\vec{k}_{1\perp} - \vec{k}_{2\perp} - 2\vec{r}_\perp + m) \gamma_\nu u(r_2 - r_1) \\ & \times \int_0^{2\omega} dk_{2-} \int_{-k_{2-}}^0 dk_{1-} (k_{1-} + k_{2-}) \{ k_{1-} [-C_1(2\omega - k_{2-})^{-1} + C_2(k_{1-} + k_{2-})^{-1}] - \vec{k}_{1\perp}^2 - \lambda^2 + i\epsilon \}^{-1} \\ & \times \{ k_{1-} [-2\omega - C_1(2\omega - k_{2-})^{-1} + C_2(k_{1-} + k_{2-})^{-1}] - (\vec{k}_{1\perp} + \vec{r}_\perp)^2 - m^2 + i\epsilon \}^{-1} \\ & \times \{ (k_{1-} + k_{2-}) [-2\omega + C_2(k_{1-} + k_{2-})^{-1}] - (\vec{k}_{1\perp} + \vec{k}_{2\perp} + \vec{r}_\perp)^2 - m^2 + i\epsilon \}^{-1} \\ & \times [(k_{1-} + k_{2-} - 2\omega) C_2(k_{1-} + k_{2-})^{-1} - (\vec{k}_{2\perp} + \vec{r}_\perp)^2 - m^2 + i\epsilon]^{-1} \\ & \times [k_{2-} C_1(2\omega - k_{2-})^{-1} - \vec{k}_{2\perp}^2 - \lambda^2 + i\epsilon]^{-1}. \end{aligned} \quad (9.9)$$

The only edge of the triangle (9.6) which gives a contribution to (9.9) of order $\ln^2 s$ (for the real part) is

$$0 < -k_{1-} \ll k_{2-} \ll 2\omega. \quad (9.10)$$

Thus (9.9) reduces to

$$\begin{aligned} \mathcal{G}_A \doteq & -g^6 \int d^2\vec{k}_{1\perp} (2\pi)^{-3} \int d^2\vec{k}_{2\perp} (2\pi)^{-3} s \bar{u}(r_3 - r_1) \gamma_\mu (-\vec{k}_{1\perp} - \vec{k}_{2\perp} - 2\vec{r}_\perp + m) \gamma_\nu u(r_2 - r_1) \\ & \times (\vec{k}_{1\perp}^2 + \lambda^2)^{-1} (\vec{k}_{2\perp}^2 + \lambda^2)^{-1} [(\vec{k}_{1\perp} + \vec{k}_{2\perp} + 2\vec{r}_\perp)^2 + m^2]^{-1} \\ & \times \int_0^{2\omega} dk_{2-} (-2\omega k_{2-} + C_2 - C_3)^{-1} \int_{-k_{2-}}^0 dk_{1-} [-2\omega k_{1-} - (\vec{k}_{1\perp} + \vec{r}_\perp)^2 - m^2 - i\epsilon]^{-1}. \end{aligned} \quad (9.11)$$

The smallest integration variable is k_{1-} and there is a pole on the k_{1-} path of integration as $\epsilon \rightarrow 0$. Hence (9.11) has an imaginary part and we obtain

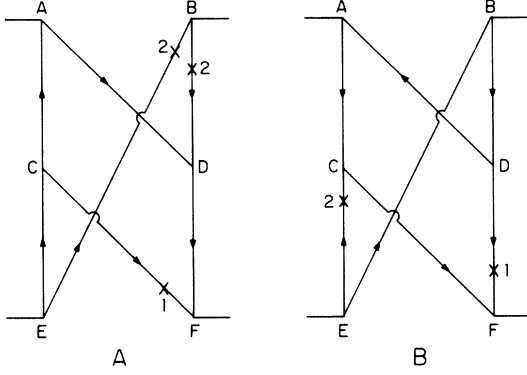


FIG. 10. The two momentum-flow diagrams for Feynman diagram 4. In both momentum-flow diagrams the first loop momentum is $ADFC A$ and the second loop momentum is $ADBECA$.

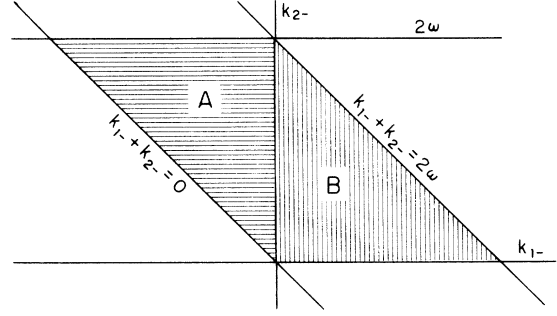


FIG. 11. The region in k_{1-}, k_{2-} space that gives a nonvanishing contribution to the sixth-order diagram 4. The subregions A and B correspond to momentum flow diagrams A and B.

$$\mathcal{G}_A \doteq -g^6 \frac{1}{2} (\ln^2 s - 2\pi i \ln s)$$

$$\begin{aligned} & \times \int d^2 \vec{k}_{1\perp} (2\pi)^{-3} d^2 \vec{k}_{2\perp} (2\pi)^{-3} \bar{u}(r_3 - r_1) \gamma_\mu (-\vec{k}_{1\perp} - \vec{k}_{2\perp} - 2\vec{F}_1 + m) \gamma_\nu u(r_2 - r_1) \\ & \times (\vec{k}_{1\perp}^2 + \lambda^2)^{-1} (\vec{k}_{2\perp}^2 + \lambda^2)^{-1} [(\vec{k}_{1\perp} + \vec{k}_{2\perp} + 2\vec{F}_1)^2 + m^2]^{-1}. \end{aligned} \quad (9.12)$$

B. Diagram B

We find from Fig. 10 that for diagram B the momentum region is (see Fig. 11)

$$0 < k_{1-}, \quad 0 < k_{2-}, \quad k_{1-} + k_{2-} < 2\omega \quad (9.13)$$

and that the poles to close on are

$$k_{2+} = k_{1-}^{-1} C_5, \quad (9.14a)$$

$$k_{1+} = -k_{2+} + C_6 (2\omega - k_{1-} - k_{2-})^{-1}, \quad (9.14b)$$

with

$$C_5 = \vec{k}_{2\perp}^2 + \lambda^2 - i\epsilon, \quad (9.15a)$$

$$C_6 = (\vec{k}_{1\perp} + \vec{k}_{2\perp} + \vec{F}_1)^2 + m^2 - i\epsilon. \quad (9.15b)$$

Thus we find

$$\begin{aligned} \mathcal{G}_B \doteq & -g^6 (2\pi i)^2 \int d^2 \vec{k}_{1\perp} (2\pi)^{-4} d^2 \vec{k}_{2\perp} (2\pi)^{-4} (2\omega)^3 \bar{u}(r_3 - r_1) \gamma_\mu (-\vec{k}_{1\perp} - \vec{k}_{2\perp} - 2\vec{F}_1 + m) \gamma_\nu u(r_2 - r_1) \\ & \times \int_0^{2\omega} dk_{2-} \int_0^{2\omega - k_{2-}} dk_{1-} k_{2-}^{-1} \{ k_{1-} [-k_{2-}^{-1} C_1 + C_2 (2\omega - k_{1-} - k_{2-})^{-1}] - \vec{k}_{1\perp}^2 - \lambda^2 + i\epsilon \}^{-1} \\ & \times \{ k_{1-} [-2\omega - k_{2-}^{-1} C_1 + C_2 (2\omega - k_{1-} - k_{2-})^{-1}] - (\vec{k}_{1\perp} + \vec{F}_1)^2 - m^2 + i\epsilon \}^{-1} \\ & \times \{ (k_{1-} + k_{2-}) [-2\omega + C_2 (2\omega - k_{1-} - k_{2-})^{-1}] - (\vec{k}_{1\perp} + \vec{k}_{2\perp} + \vec{F}_1)^2 - m^2 + i\epsilon \}^{-1} \\ & \times [(k_{1-} + k_{2-}) C_2 (2\omega - k_{1-} - k_{2-})^{-1} - (\vec{k}_{1\perp} + \vec{k}_{2\perp} + 2\vec{F}_1)^2 - m^2 + i\epsilon]^{-1} \\ & \times [(k_{2-} - 2\omega) C_2 k_{2-}^{-1} - (\vec{k}_{2\perp} + \vec{F}_1)^2 - m^2 + i\epsilon]^{-1}. \end{aligned} \quad (9.16)$$

It may be verified that the only edge of (9.13) that contributes to leading order is

$$0 < k_{1-} \ll k_{2-} \ll 2\omega. \quad (9.17)$$

We then find that

$$\begin{aligned}
\mathcal{G}_B \doteq & -g^6(2\omega) \int d^2 \vec{k}_{1\perp} (2\pi)^{-3} d^2 \vec{k}_{2\perp} (2\pi)^{-3} \bar{u}(r_3 - r_1) \gamma_\mu (-\vec{k}_{1\perp} - \vec{k}_{2\perp} - 2\vec{r}_\perp + m) \gamma_\nu u(r_2 - r_1) \\
& \times (\vec{k}_{1\perp}^2 + \lambda^2)^{-1} (\vec{k}_{2\perp}^2 + \lambda^2)^{-1} [(\vec{k}_{1\perp} + \vec{k}_{2\perp} + 2\vec{r}_\perp)^2 + m^2]^{-1} \\
& \times \int_0^{2\omega} dk_{2-} \int_0^{k_{2-}} dk_{1-} k_{2-}^{-1} [-2\omega k_{1-} - (\vec{k}_{1\perp} + \vec{r}_\perp)^2 - m^2 + i\epsilon]^{-1}.
\end{aligned} \tag{9.18}$$

In the k_{1-} (smallest variable) integration there is no pole on the integration path as $\epsilon \rightarrow 0$. Therefore the integral is real and we obtain

$$\begin{aligned}
\mathcal{G}_B \doteq & g^6 \frac{1}{2} \ln^2 s \int d^2 \vec{k}_{1\perp} (2\pi)^{-3} d^2 \vec{k}_{2\perp} (2\pi)^{-3} \bar{u}(r_3 - r_1) \gamma_\mu (-\vec{k}_{1\perp} - \vec{k}_{2\perp} - 2\vec{r}_\perp + m) \gamma_\nu u(r_2 - r_1) \\
& \times (\vec{k}_{1\perp}^2 + \lambda^2)^{-1} (\vec{k}_{2\perp}^2 + \lambda^2)^{-1} [(\vec{k}_{1\perp} + \vec{k}_{2\perp} + 2\vec{r}_\perp)^2 + m^2]^{-1}.
\end{aligned} \tag{9.19}$$

C. Summation of momentum-flow diagrams

It remains to add (9.12) and (9.19). The real parts cancel but the imaginary part does not. Therefore

$$\begin{aligned}
\mathfrak{N}_{4\nu}^{(2)}(s, r_1) \doteq & g^2 \pi i \ln s \int d^2 \vec{k}_{1\perp} (2\pi)^{-3} d^2 \vec{k}_{2\perp} (2\pi)^{-3} \bar{u}(r_3 - r_1) \gamma_\mu (-\vec{k}_{1\perp} - \vec{k}_{2\perp} - 2\vec{r}_\perp + m) \gamma_\nu u(r_2 - r_1) \\
& \times (\vec{k}_{1\perp}^2 + \lambda^2)^{-1} (\vec{k}_{2\perp}^2 + \lambda^2)^{-1} [(\vec{k}_{1\perp} + \vec{k}_{2\perp} + 2\vec{r}_\perp)^2 + m^2]^{-1}.
\end{aligned} \tag{9.20}$$

These integrals over transverse momenta converge at large momenta so the cutoff k_{\max} may be removed.

We emphasize that this calculation is not accurate enough to compute the real part of the sixth-order amplitude to order $\ln s$.

Finally, we may add (9.20) to (7.2) to obtain the complete leading-order contribution to both the real and the imaginary parts of the sixth-order backward Compton amplitude:

$$\begin{aligned}
\mathfrak{N}_{\mu\nu}^{(2)}(s, r_1) \doteq & g^2 \frac{1}{2} (\ln^2 s - 2\pi i \ln s) \bar{u}(r_3 - r_1) \gamma_\mu \frac{1}{2\vec{r}_\perp + m} [\alpha(2\vec{r}_\perp)]^2 \gamma_\nu u(r_2 - r_1) \\
& + g^4 \pi i \ln s \int \frac{d^2 \vec{k}_{2\perp}}{(2\pi)^3} (\vec{k}_{2\perp}^2 + \lambda^2)^{-1} \bar{u}(r_3 - r_1) \gamma_\mu \frac{1}{\vec{k}_{2\perp} + 2\vec{r}_\perp + m} \alpha(\vec{k}_{2\perp} + 2\vec{r}_\perp) \gamma_\nu u(r_2 - r_1),
\end{aligned} \tag{9.21a}$$

where $\alpha(2\vec{r}_\perp)$ is given by (2.25).

An identical analysis may be carried out for pair annihilation and we obtain

$$\begin{aligned}
\bar{\mathfrak{N}}_{\mu\nu}^{(2)}(s, r_1) \doteq & g^2 \frac{1}{2} \ln^2 s \bar{v}(r_3 + r_1) \gamma_\mu \frac{1}{2\vec{r}_\perp + m} [\alpha(2\vec{r}_\perp)]^2 \gamma_\nu u(r_2 - r_1) \\
& - g^4 \pi i \ln s \int \frac{d^2 \vec{k}_{2\perp}}{(2\pi)^3} (\vec{k}_{2\perp}^2 + \lambda^2)^{-1} \bar{v}(r_3 + r_1) \gamma_\mu \frac{1}{\vec{k}_{2\perp} + 2\vec{r}_\perp + m} \alpha(\vec{k}_{2\perp} + 2\vec{r}_\perp) \gamma_\nu u(r_2 - r_1).
\end{aligned} \tag{9.21b}$$

ACKNOWLEDGMENT

We wish to thank Professor H. Cheng for many useful discussions.

*Work supported in part by the U. S. Energy Research and Development Administration under Contract No. AT(11-1)-3227.

†Alfred P. Sloan fellow. Work supported in part by the National Science Foundation under Grant No. DMR73-07565 A01.

¹H. Cheng and T. T. Wu, Phys. Rev. **140**, B465 (1965).

²B. McCoy and T. T. Wu, preceding paper, Phys. Rev. D **13**, 369 (1976).

³M. Gell-Mann, M. L. Goldberger, F. E. Low, E. Marx, and F. Zachariasen, Phys. Rev. **133**, B145 (1964).

⁴H. Cheng and T. T. Wu, Phys. Rev. **182**, 1899 (1969).

⁵H. Cheng and T. T. Wu, Phys. Rev. **182**, 1873 (1969).